A subwavelength slit as a quarterwave retarder

Johan Bosman

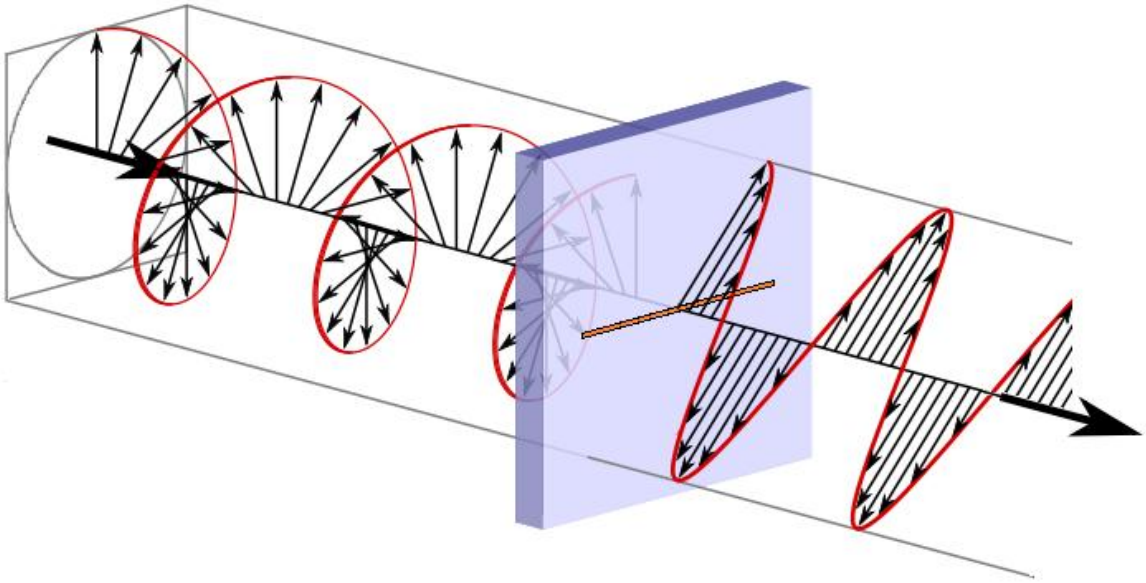

Table of contents

Abstract 3

Introduction 3

Theory 5
- *Model* 5
- *Stokes analysis* 7

Materials & Methods 8
- *Creating the desired input polarization* 8
- *Properties of the sample* 9
- *Milling depth of the slits* 9
- *Alignment* 10

Results 11
- *Full Stokes analysis* 11
- *Comparison of different effective milling depths* 13
- *Dichroism* 14
- *Phase shift* 15

Discussion 16
- *Alignment process* 16

Conclusion 16

References 17

Abstract

We measured the polarization-dependent transmission of subwavelength slits in a gold film as a function of its width. Measurements show strong dichroism and birefringence. Surprisingly, the TE-polarization transmission only vanishes at widths much smaller than half a wavelength, while the transmission TM-polarization is reduced by the excitation of surface plasmons. We used the slit's dichroism and birefringence to create a quarter-wave retarder.

Introduction

The inspiration for this experiment found its origin in a research project that focused on something different: the properties and coupling of surface plasmons[1]. Although there are various ways to excite surface plasmons, many experiments that were performed used subwavelength slits in metal films to excite the surface plasmons.

The research also contained some measurements of the light that was transmitted through the subwavelength slits, which yielded some unexpected results, see Figure 1. For these slits, which are long in one dimension and subwavelength in the other, elementary waveguide theory predicts that when they are modeled as infinitely long slits they would act as a perfect polarizer when the slit width w is less than half the wavelength of the incident light.

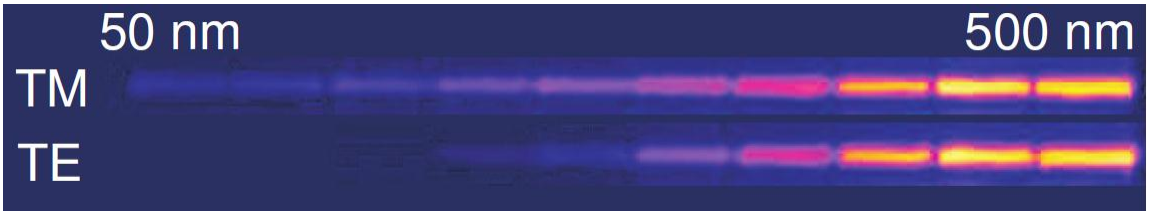

Figure 1: Transmission of the TE and TM mode through various subwavelength slits, see Figure 6.4a of Ref. 1. The slits' widths increase stepwise from 50 nm to 500 nm. The transmission of the TE mode is still visible well below the cutoff width.

When modeled as infinitely long slits, elementary waveguide theory shows there are two modes: transverse electric (TE), with its electric field vector parallel to the long axis of the slit, and transverse magnetic (TM), with its electric field vector perpendicular to the long axis of the slit. In an ideal slit, the metal is assumed to be perfect which means that parallel component of the electric field must be zero at the metal walls of the slit. This implies that the TE mode incident on this slit will not be transmitted when the width of the slit is less than half the wavelength, often referred to as the cutoff width, while the TM mode can propagate unimpeded through the slit. This suggests that very narrow slits ($w < \lambda/2$) in metal films would act as perfect polarizers.

Figure 1 shows that the TE mode is not only transmitted far beyond cutoff width, but that the cutoff is more gradual than the theory suggests. Measurements also showed that the two modes encountered a phase difference during the transmission through the slit, indicating that the slit has some birefringent properties.
This experiment further explored these properties of subwavelength slits and employed these properties to create a subwavelength slit which acts as a quarter-wave retarder.

Theory

Model

To explain our measurements we model the slit as a simple but non-ideal waveguide. The slits used for the experiment, length *l* and width *w* (with $l > w$), have a large length/width ratio, so we modeled it with $l \to \infty$: a step index planar waveguide. The model consists of an infinitely long slit of width *w* in a thin gold layer with metal permittivity ε and thickness *d* on a glass substrate. The thin titanium adhesion layer present in the sample between the gold film and the glass substrate is ignored in this model. See Figure 2.

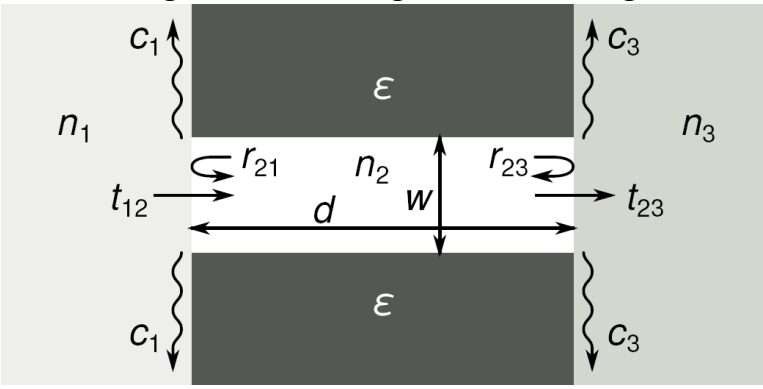

Figure 2: Cross-section of our model slit with the relevant physical quantities shown, see Figure 5 of Ref. 2.

Inside the waveguide the solutions to the Maxwell equations separate into two modes, TE and TM. Each of these modes has its own complex propagation constant, β_{TE} and β_{TM}, which can only be calculated numerically[3].

The effective index of the subwavelength slit is different than the index of the material itself in bulk. This effective mode index for the waveguide, n^{eff}, can be calculated with the propagation constants:

$$n_i^{eff} = \frac{\beta_i}{k_0}; k_0 = \frac{2\pi}{\lambda}; i = TE, TM \qquad \textbf{(1)}$$

n_2 must be substituted with this effective mode index to calculate the transmission through the slit. As n_i^{eff} is unequal to the index of the media at the front and the back of the slit for both modes, the incident light will be partially reflected at the air-waveguide and the waveguide-glass interface. These transmission and reflection coefficients (t_{12}, t_{23}, r_{21} and r_{23}, see Figure 2) can be calculated for both modes with the Fresnel equations at normal incidence (Eqs. (2) and(3)). As the effective mode index of the waveguide is different for the TE and TM mode, the transmission and reflection coefficients will also be different for both modes.

$$r_{ab} = \frac{n_a - n_b}{n_a + n_b} \quad \textbf{(2)}$$

$$t_{ab} = \frac{2n_a}{n_a + n_b} \quad \textbf{(3)}$$

Although this simplification in the model avoids calculating the overlap integrals between the guided mode and the modes outside the waveguide, it still describes the phenomena quite well.
The next step in the model is to treat the waveguide as a Fabry-Pérot interferometer. The formula for the complex transmission through a Fabry-Pérot interferometer of length *d* is given by:

$$T_i = \frac{n_3}{n_1}\left|t^i_{123}\right|^2 ; t^i_{123} = \frac{t_{12}t_{23}e^{i\beta_i d}}{1 - r_{21}r_{23}e^{2i\beta_i d}} ; i = \text{TE, TM} \quad \textbf{(4)}$$

The complex transmission also contains the phase shift picked up because of the transmission through the slit and can be used to calculate the phase difference between the TM and TE mode after passing through the slit:

$$\Delta\varphi = \arg(t^{TM}_{123}) - \arg(t^{TE}_{123}) \quad \textbf{(5)}$$

The TM mode of the waveguide also couples to surface plasmons on both interfaces of the waveguide, which must also be taken into account and can be calculated by Eq. (20) of Ref. 4, which gives an approximate analytical model. The TE mode does not couple to surface plasmons. This results in the following transmission coefficients of the TE and TM mode:

$$T_{TE} = \frac{n_3}{n_1}\left|t^{TE}_{123}\right|^2 \quad \textbf{(6)}$$

$$T_{TM} = \frac{n_3}{n_1}\left|t^{TM}_{123}\right|^2 - 2\left|c_1\right|^2 - 2\left|c_3\right|^2 \quad \textbf{(7)}$$

For the transmission into the glass substrate, the slit acts as a subwavelength source due to its small width. The source profile is different for the TE and TM modes. The scattering profile is proportional to the Fourier transform of the source profile and therefore the scattering profile is different for the TE and TM mode**.** As our detection system has a numerical aperture (NA) less than 1, not all transmitted light can be captured and therefore we must adjust the results to compensate for the unequal losses.

Stokes analysis

The polarization analysis of the transmitted light consists of measuring all four Stokes parameters for each slit with a quarter-wave plate and a linear polarizer. We used the following definition for the Stokes parameters:

- S_0 is the total intensity,
- S_1 is the intensity of the horizontal component (TE) minus the vertical component (TM),
- S_2 is the intensity of the diagonal component (45° clockwise) minus the anti-diagonal component (45° counter-clockwise) and
- S_3 is the intensity of the right-handed circular component minus the left-handed circular component.

We've used the normalized Stokes parameters in the results, as the transmitted light is fully polarized: $s_1 = S_1/S_0$, $s_2 = S_2/S_0$, $s_3 = S_3/S_0$, each ranging from -1 to +1.

The relation between the normalized Stokes parameters, s_1, s_2 and s_3, the transmission coefficients, T_{TM} and T_{TE}, the phase shift, $\Delta\varphi$, and the initial phase difference of the incident light, ψ, are shown in Eqs. (8) to (10).

$$s_1 = -\frac{T_R E_{TM}^2 - E_{TE}^2}{T_R E_{TM}^2 + E_{TE}^2}; T_R = \frac{T_{TM}}{T_{TE}} \quad \textbf{(8)}$$

$$s_2 = \frac{2\sqrt{T_R}\, E_{TM} E_{TE}}{T_R E_{TM}^2 + E_{TE}^2} \cos(\Delta\varphi - \psi) \quad \textbf{(9)}$$

$$s_3 = -\frac{2\sqrt{T_R}\, E_{TM} E_{TE}}{T_R E_{TM}^2 + E_{TE}^2} \sin(\Delta\varphi - \psi) \quad \textbf{(10)}$$

Materials & methods

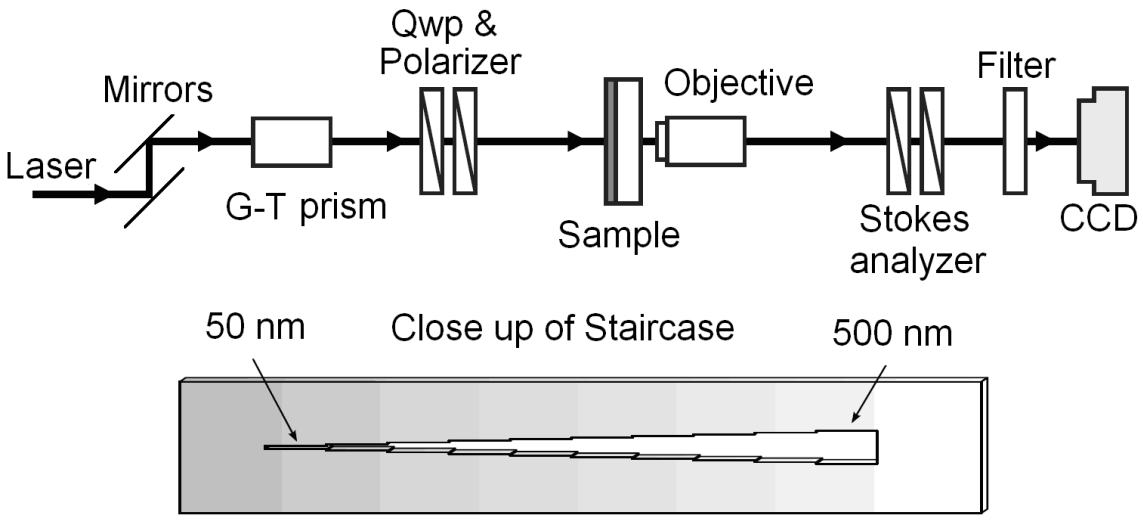

Figure 3: Schematic of the experiment, an expansion of Figure 5 of Ref. 2. The laser beam illuminates the sample on the gold side, with its polarization controlled by a (G-T) prism, a QWP and a polarizer under computer control. The transmitted light is filtered and imaged with an objective on the CCD camera. The Stokes analyzer consists of a polarizer and a quarter-wave plate, both under computer control to measure any particular polarization.

In the experiment, of which the schematic is shown in Figure 3, we illuminated the sample with a laser beam at λ = 830 nm. The laser used was a diode laser (Thorlabs LPS-830-FC), connected to a single mode fiber and the beam was aligned with two infrared mirrors (broadband coating, λ = 700-900 nm). The width of the laser beam was 4 mm, so that effectively the whole sample was illuminated homogeneously with a flat wavefront. The light transmitted through the slits was imaged on the CCD camera (Apogee Alta U1) with a 0.65 NA microscope objective. As the measurements were sensitive to noise from external light sources, we placed a longpass filter (λ_c = 665 nm, Thorlabs FGL665) in front of the CCD. All measurements were performed in a dark room, and part of the setup, from the objective to the camera, was shielded with black cardboard. The sample was fixed on an xyz-translation mount and the polarizer and Stokes analyzer were on motorized rotation-stages to get an accurate alignment and to automate the measurement process.

Creating the desired input polarization

After the laser beam is reflected by the mirrors, it passes through a Glan-Thompson prism to create a stable purely linearly polarized beam, as the polarization of the laser beam was unpredictable and changed erratically when the fiber was touched. The beam then passes through a quarter-wave plate (λ = 826 nm) and a polarizer to create the desired input polarization.

To create any of the linear polarizations (horizontal, vertical and (anti-)diagonal), the beam passes through the quarter-wave plate first, creating a circular polarization. Then it passes through the polarizer, mounted on a computer controlled rotation stage. The

polarizer is set to the desired angle, creating either horizontal, vertical or (anti-) diagonal polarization.
To create the circular input polarization, the laser beam passes through the computer controlled polarizer first and then through the quarter-wave plate. The polarizer is set to create a linear polarization at 45° relative to the fast axis of the quarter-wave plate, which in turn transforms the polarization into circular polarization. To create the opposite circular polarization, the computer controlled polarizer is rotated 90°.

Properties of the sample

The sample consists of a 200 nm thick gold film deposited on a 0.5 mm thick Schott D263T borosilicate glass substrate. In between the gold film and the substrate, there is a 10 nm titanium adhesion layer. This layer damps the surface plasmons, ensuring that they only propagate on the glass-air interface. On the sample there are multiple sets of slits milled next to each other into the gold film using a focused ion beam, with each set a few millimeters apart. One set of slits consists of ten slits, each 10 µm long and widths increasing from 50 nm to 500 nm with steps of 50 nm, also called a 'staircase'. Figure 3 shows an example of a staircase.

Milling depth of the slits

Because the milling depths of the focused ion beam are configured for glass as opposed to the much softer gold the ion beam is milling in, it had to be determined what milling depth would yield the best slits. In Figure 4 you can see the crosscuts through test slits with the same width and different depths. The lengths in Figure 4 are the milling depths created by the ion beam if it were used on glass, called 'effective milling depth', and not the actual depth of the slit. Figure 4 shows that the gold is milled through at an effective milling depth between 20 and 30 nm. Also the side walls of the test-slits are not completely perpendicular to the surface but sloped by a few degrees, which is more visible at lower milling depths. To find which milling depth would yield the best results, four staircases were milled into the actual sample, with effective milling depths 20 nm, 40 nm, 60 nm, and 80 nm. The transmission through the slits of the staircase with 20 nm effective milling depth proved to be much lower than that of the other three staircases, meaning that the ion beam had not milled through the gold film completely. Therefore this staircase was not fit for proper measurements and was not included in the experiment.

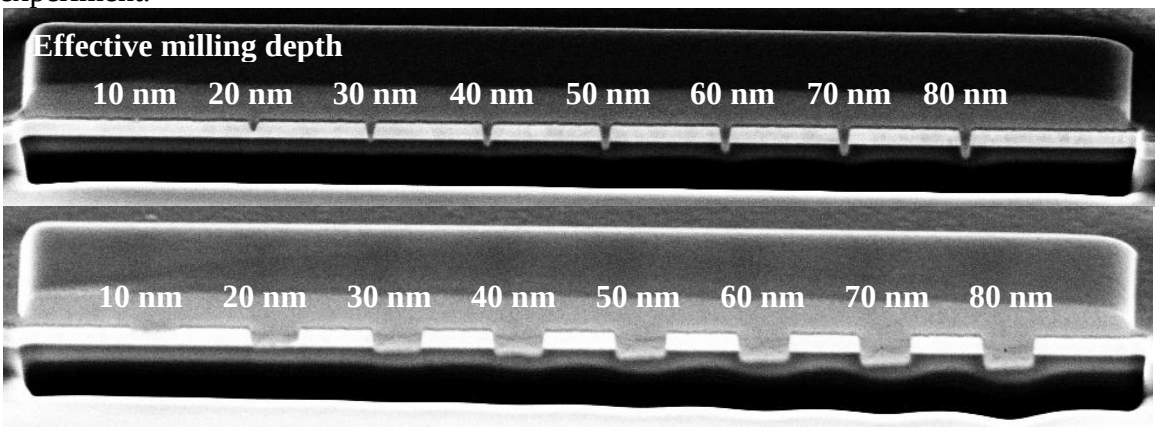

Figure 4: Crosscuts of test slits with a constant width and different milling depths, used to examine the milling depths, see Ref. 5. The slits in the top picture are 50 nm wide, the ones in bottom picture are 500 nm wide.

Alignment

First we aligned all optical elements with each other and then we placed the sample into the setup. To align the axis of the optical elements with the axis of the sample, we measured s_1 over a few degrees at the three narrowest slits with TE input polarization, as seen in Figure 5. If there is a small deviation in the angle of the axis, then the input polarization won't be in the TE direction but rotated slightly, resulting in a polarization with a large TE component, but with also a minor TM component. As the transmission ratio of the TM component is a few orders of magnitude greater than the transmission ratio of the TE component for these small slit widths, the transmitted light will have a relatively large TM component. This will result in a normalized Stokes parameter s_1 much smaller than 1. This measurement also serves to check whether the slits are properly shaped: If the walls of the slit are not parallel but converge on one end, this will show up in this alignment process. In this case there would be 2 sets of eigenmodes instead of only 1 set of eigenmodes: there would be a different TE (and TM mode) for both walls, which would yield two peaks in Figure 5, both (substantially) lower than 1.

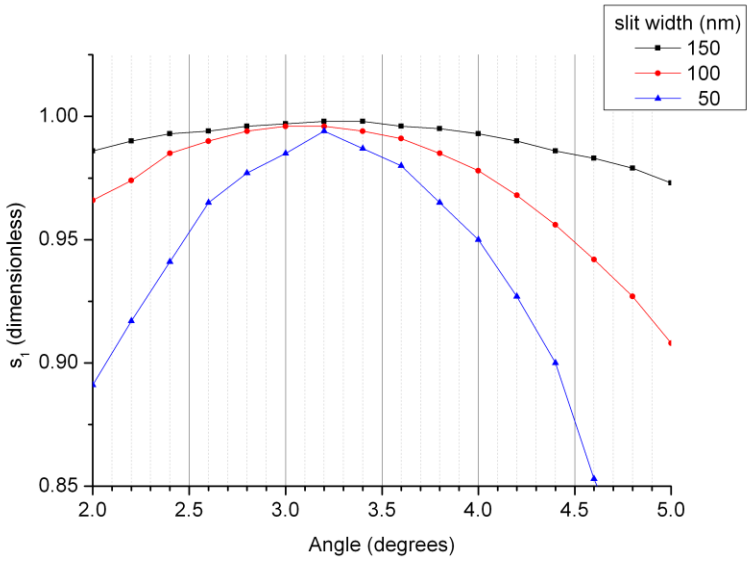

Figure 5: Normalized Stokes parameter s_1 for TE (horizontal) input polarization of the three narrowest slits. All three slits show one peak at the same angle, demonstrating that they are properly shaped.

As all three slits show one peak at 3.2° in Figure 5, the following things could be determined:

- As all three slits show one peak, each one is properly shaped.
- They all have the peak that the same angle, demonstrating that the axis of each slit is parallel to the axis of the other slits.
- The axes of the slits are rotated by 3.2° with respect to the optical elements in the setup. This was adjusted for in the subsequent measurements.

Results

Full Stokes analysis

The full Stokes analysis of the staircase that yielded the best results, the staircase with an effective milling depth of 60 nm, is shown in Figure 6. The full Stokes analysis consists of the Stokes analysis of the transmitted light for each of the six basic Stokes input polarizations ($s_{1,2,3} = \pm 1$). As seen in figures 6a-b, the measurements confirm that TE and TM polarizations are the two eigenpolarizations of the slits.

Figures 6c-f show that at the narrowest slit widths, s_1 will converge to -1 and s_2 and s_3 to 0 for any input polarization except the eigenpolarizations, showing that the transmitted polarization for the narrowest slits is dominated by the TM mode. This is because the TM polarization is transmitted more easily through the smallest slits compared to the TE polarization.

When looking more closely at Figure 6c, the Stokes analysis with diagonally linear polarized incident light ($s_2 = +1$), you can see that for slit width decreasing from 500 nm to 250 nm s_2 goes from almost 1 to approximately 0, while s_3 goes from approximately -0.5 to almost 1. The transmitted light becomes more and more elliptically polarized with decreasing slit width, while almost becoming circular around 250 nm. While the transmitted light becomes more elliptically polarized with slit width decreasing from 500 nm to 250 nm, the main axis of the polarization ellipse remains oriented along the same axis as the incident light. When the slit width decreases further from 250 nm, the axis of the polarization ellipse rapidly shifts to orient itself vertically, whilst the polarization becomes more linear. Ultimately the transmitted light becomes purely TM polarized around $w = 50$ nm. Figure 6d, the Stokes analysis with *anti*-diagonally linear polarized incident light ($s_{1,2,3} = (0,-1,0)$), shows the same behavior as in Figure 6c, with the signs of s_2 and s_3 flipped.

In Figure 6e-f a similar process happens: For slit widths decreasing from 500 nm to 250 nm, the transmitted light goes from elliptically polarized to more and more linearly polarized. When the slit width decreases further from 250 nm, the transmitted light becomes a little bit elliptically polarized again, before ending purely TM polarized at $w = 50$ nm.

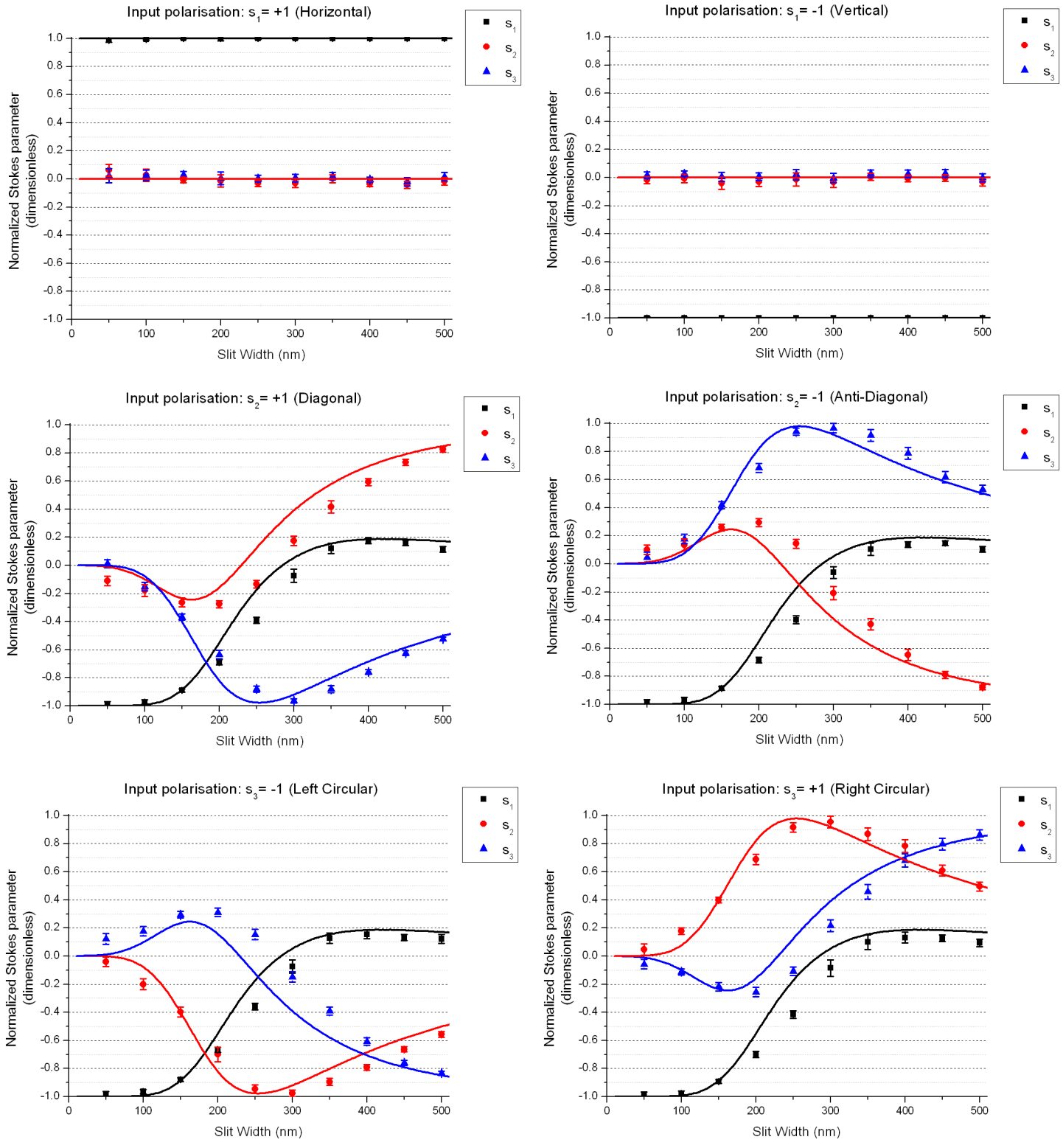

Figure 6: Normalized Stokes parameters of the light transmitted through the slit for illumination with (a) horizontal linear polarization (s_1 = +1), (b) vertical linear polarization (s_1 = -1), (c) diagonal linear polarization (s_2 = +1), (d) anti-diagonal linear polarization (s_2 = -1), (e) right-handed circular polarization (s_3 = +1), (f) left-handed circular polarization (s_3 = -1). The points represent the measured Stokes parameters, while the lines represent the results of our model.

Comparison of different effective milling depths

The full Stokes analysis of the staircases with an effective milling depth of 40 nm and 80 nm yield very similar results to the staircase in Figure 6, though with some deviations in certain areas. For a close inspection of some of the differences between the staircases, the measurements of the transmission of input polarization $s_2 = +1$ of the three staircases are compared in Figure 7. s_1 looks quite consistent for all three staircases: the slope, the start of the rapid decline and the point where s_1 reaches -1 show no substantial differences. s_2 for the 80 nm depth staircase, however, deviates significantly from the model and the other staircases. With decreasing slit width s_2 does not decrease as rapidly as at the other staircases but follows the model, although it does not reach a minimum around 150-200 nm before converging to 0 when the slit width decreases to 50 nm. For the 80 nm depth staircase, s_3 also deviates from the 60 nm and 40 nm depth as seen in Figure 7c, but is more consistent with the model for $w \geq 250$ nm, and less consistent for $w < 250$ nm. For the overall behavior of s_3, the other two staircases are qualitatively more consistent with the model.

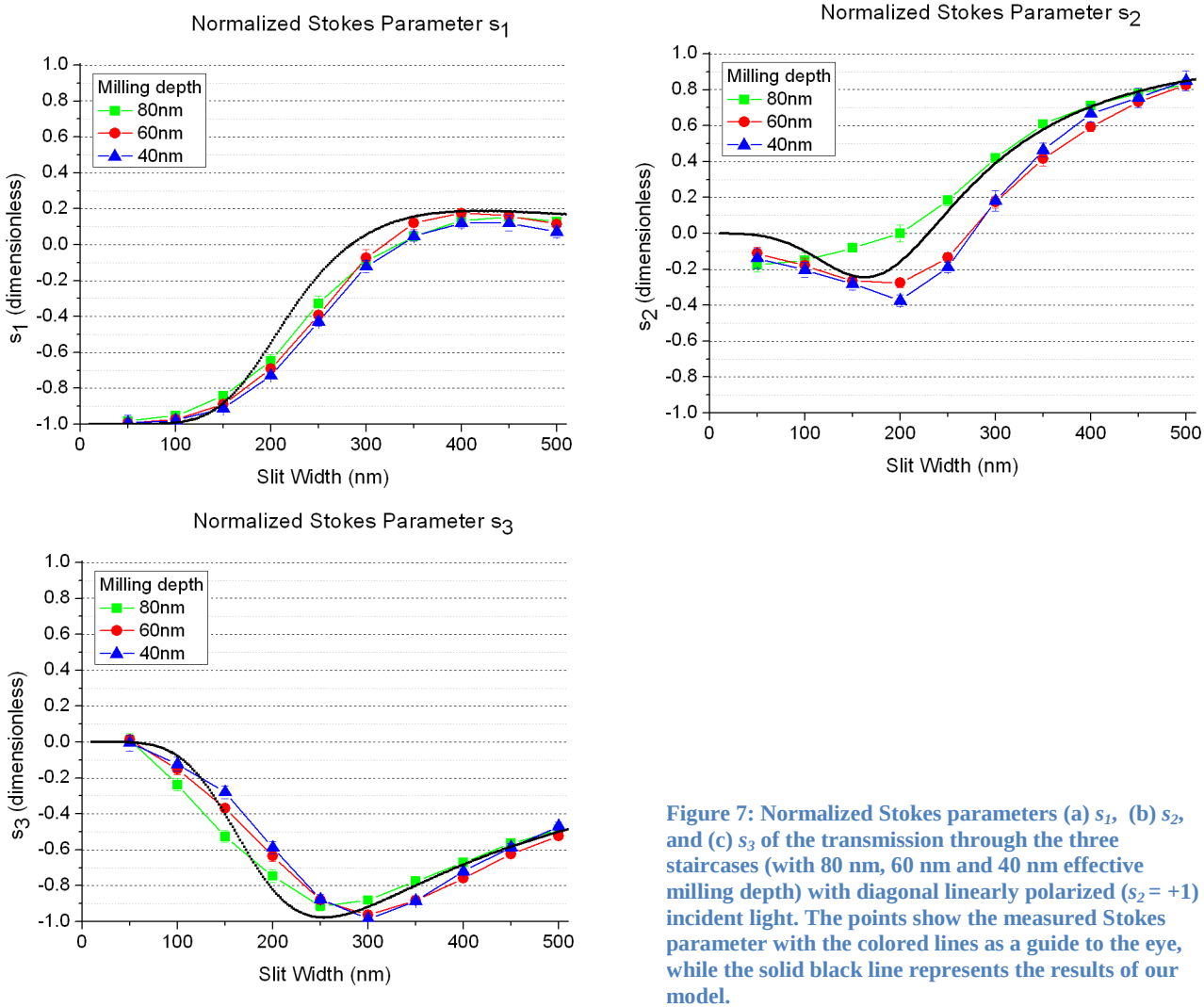

Figure 7: Normalized Stokes parameters (a) s_1, (b) s_2, and (c) s_3 of the transmission through the three staircases (with 80 nm, 60 nm and 40 nm effective milling depth) with diagonal linearly polarized ($s_2 = +1$) incident light. The points show the measured Stokes parameter with the colored lines as a guide to the eye, while the solid black line represents the results of our model.

Dichroism

Measurements on the dichroism of the subwavelength slit are shown in Figure 8. For the three staircases, the transmission of the TE and TM polarizations through the slits were measured, and normalized to the transmission of the TE-polarized light through a 500 nm wide slit. The points in Figure 8 represent the measured data, and the solid lines represent the results of our model.

For the transmission of the TE polarization, the measurements of all three staircases follow the model quite well and show that the TE polarization is still transmitted well below $w = \lambda/2$ and only becomes negligibly small when the slit width decreases below 150 nm.

For the transmission of the TM polarization, the measurements of the staircases with an effective milling depth of 60 nm and 80 nm follow the shape of the model, though the measurements are consistently higher. When the slit width decreases from 500 nm, the transmission also decreases until it reaches a minimum at approximately w = 150 nm, where the light-surface plasmon coupling is maximal. At lower slit widths the transmission increases again. The measurement of the transmission of the TM polarization through the slits of the staircases with an effective milling depth of 40 nm is less consistent with the model. It does decrease with decreasing slit width, but instead of reaching a minimum at w = 150 nm and increasing again, it declines even further.

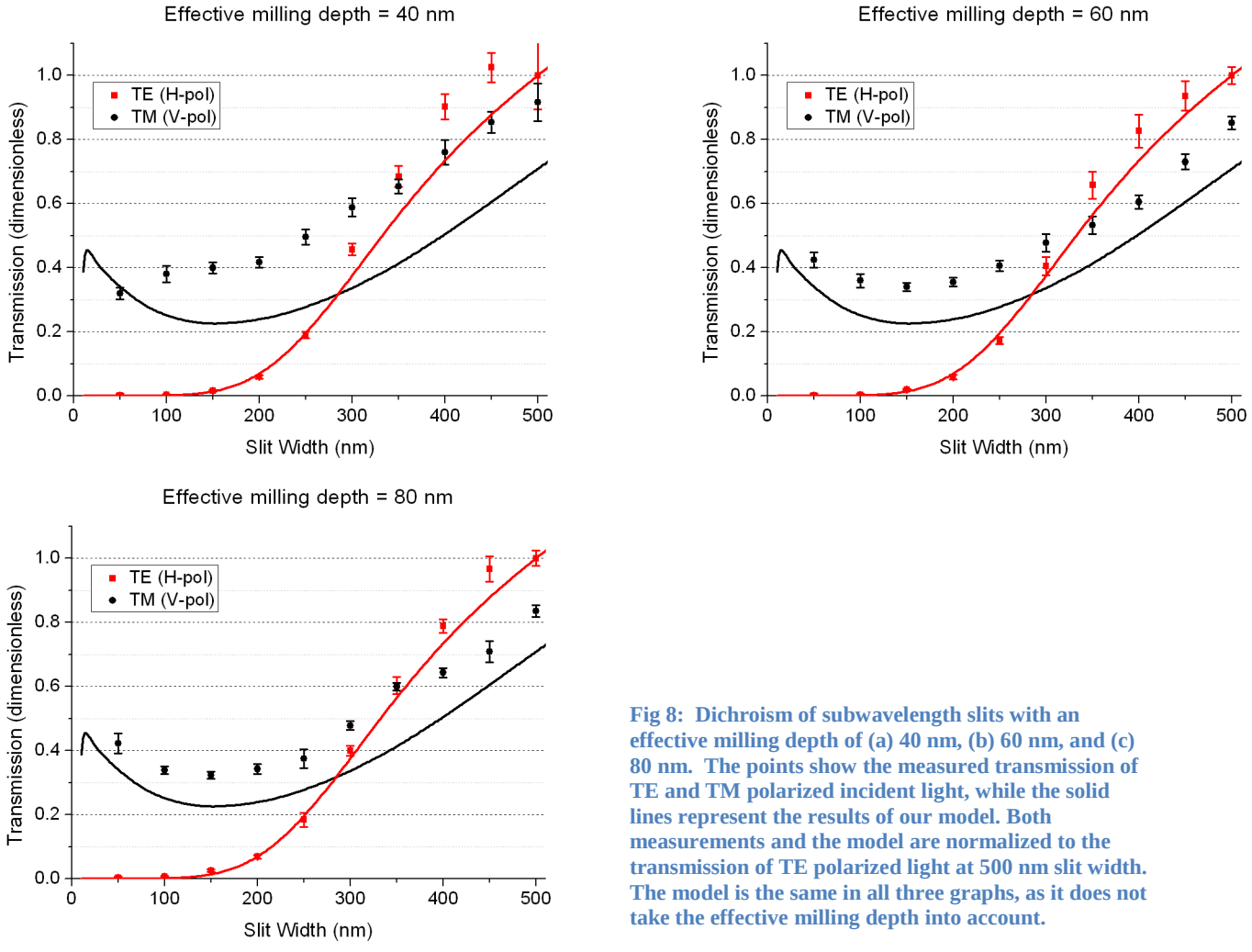

Fig 8: Dichroism of subwavelength slits with an effective milling depth of (a) 40 nm, (b) 60 nm, and (c) 80 nm. The points show the measured transmission of TE and TM polarized incident light, while the solid lines represent the results of our model. Both measurements and the model are normalized to the transmission of TE polarized light at 500 nm slit width. The model is the same in all three graphs, as it does not take the effective milling depth into account.

Phase Shift

The phase shift between the TE and TM mode of the subwavelength slits are shown in Figure 9. The phase shift is calculated from the same measurements of the full Stokes analysis of each staircase with the use of Eqs. (8) to (10). The points in Figure 9 represent the results of the measurements and the solid lines represent the results of our model.

For the phase difference between the TM and TE polarization, all three staircases follow the model quite well. When the slit width decreases, the phase difference increases almost linearly. Only when the slit with becomes very small ($w < 100$ nm) the phase difference will increase more rapidly, though in this region the transmission of TE polarization is negligible which also reduces the accuracy of the measurements there. The staircases with an effective milling depth of 40 nm and 60 nm show almost consistently a phase difference equal or greater than the model predicts, except when the slit width is below 100 nm. The staircases with an effective milling depth of 80 nm follows the model very closely for widths between 250 nm and 500 nm, but shows a smaller phase difference for $w < 250$ nm. The model predicts a $\pi/2$ phase difference at approximately 250 nm width, corresponding roughly with the measurements. At this slit width the slits act like a quarter-wave retarder, although the transmission ratio of the TE and TM polarizations are not equal there.

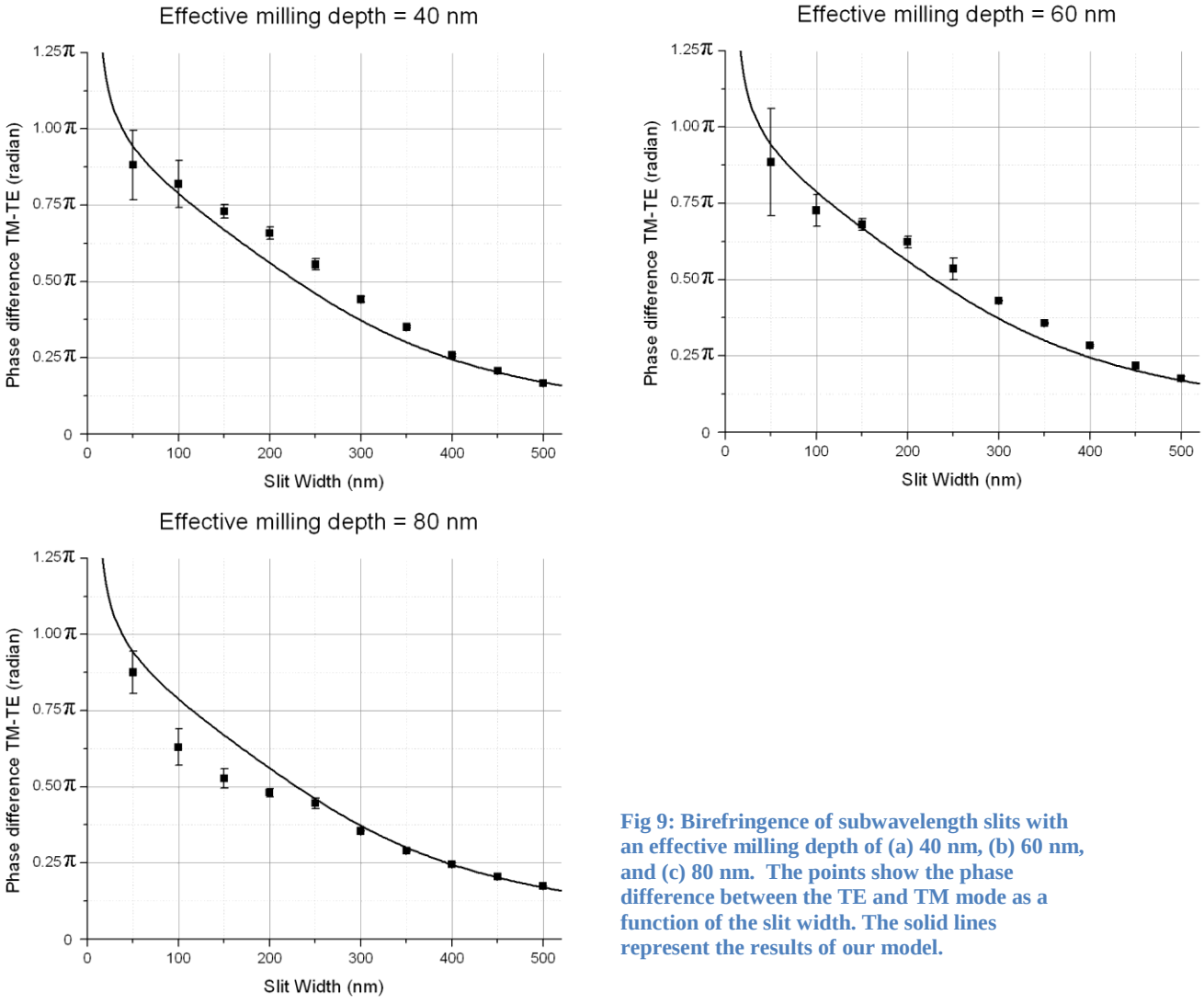

Fig 9: Birefringence of subwavelength slits with an effective milling depth of (a) 40 nm, (b) 60 nm, and (c) 80 nm. The points show the phase difference between the TE and TM mode as a function of the slit width. The solid lines represent the results of our model.

Discussion

Although the model has no fit parameters, it describes the measurements overall quite well. The three different milling depths show varying consistency with the model in all the measurements, with deviations becoming more apparent at the smaller slit widths. The 80 nm depth staircase differs most from the model at the measurements of the Stokes parameters and the phase shift for $w < 250$ nm, while the 40 nm depth staircase differs most at the measurements of the dichroism of the slits. Overall, the 60 nm depth staircase performed most consistent with the model.
These differences between the model and the staircases could be explained by the actual shape of the slits: At high milling depths the slope of slits' walls are more parallel to each other compared to lower milling depths and thus more consistent with the assumptions of the model. At the same time, the slits are also milled further into the glass substrate at higher milling depths, something the model does not account for but could which affect the measurements.

Alignment process

The alignment process shows that at the smallest slit width even very small deviations in the alignment of the axis will decrease the measurement of s_1 when illuminating the sample with horizontal polarized light, as seen in Figure 2. At the smallest slit width the transmission ratio for the TM mode of the slit is a few orders of magnitude greater than the transmission ratio of the TE mode. Therefore it was very important to minimize a possible TM component in the incident horizontal (TE) polarization to ensure proper alignment.

Conclusion

We've measured the transmission of subwavelength slits (50-500 nm) milled in a 200 nm thick gold film when illuminated with a laser ($\lambda = 830$ nm). Measurements show that the transmission of the TE mode decreases gradually with decreasing slit width, until it becomes very small at a width of about $\lambda/8$. The transmission of the TM mode does not vanish at very small slit width, but only shows a dip at a width corresponding to the maximum excitation of surface plasmons.
We've also measured the birefringence of the subwavelength slits. We showed that the TE and TM mode encounter an increasing phase difference with decreasing slit width. This phase difference passes through $\pi/2$ around 250 nm slit width. At this width the slit acts like a quarter-wave retarder, though with unequal losses for the TE and TM mode.

Our simple waveguide model used to describe these effects is very consistent with the results of our measurements. As the birefringence and dichroism depend on the properties and dimensions of the slit according to our model, future experiments could create subwavelength slits acting like a quarter-wave retarder with *equal* losses for both modes.

References

[1] Kuzmin, N. V. *Interference effects with surface plasmons*; Casimir PhD Series: Delft-Leiden, 2008-01

[2] Chimento, P. F.; Kuzmin, N. V.; Bosman, J.; Alkemade, P. F. A.; 't Hooft, G. W.; Eliel, E. R. *Optics Express* **2011**, 19, 24219–24227.

[3] Snyder, A. W.; Love, J. D. *Optical waveguide theory*; Chapman & Hall: London, 1983, 239-244

[4] Lalanne, P.; Hugonin, J. P.; Rodier, J. C. *J. Opt. Soc. Am.* A **2006**, 23, 1608–1615.

[5] Kuzmin, N. V. Labjournal, 29-1-2007